



# INTUITIVE

## INnovative Network for Training in ToUch InteractIve Interfaces

Grant agreement: #861166

H2020-MSCA-ITN-2019

Start date: 2019-10-01

End date: 2023-09-30

Deliverable reporting document

Deliverable no: 2.6		WP: 2
Deliverable name: Multi-scale model of synthetic materials mimicking tactile sensing in skin	Type: Report	Dissemination level: Public
Due Delivery date: 30 September 2022		Date delivered: 4 October 2022

### Description:

**Multi-scale model of synthetic materials mimicking tactile sensing in skin.**

**Validate in-silico model with experimental data. Use the in silico model for design and development of realistic tactile sensing skin.**

# Multi-scale model of synthetic materials mimicking tactile sensing in skin

Shashank Mishra<sup>1</sup>, Beena Rai<sup>2</sup>, Ravinder Dahiya<sup>1</sup>

<sup>1</sup>Bendable Electronics and Sensing Technologies (BEST) Group, University of Glasgow, G12 8QQ, Glasgow, UK

<sup>2</sup>TCS Research, Tata Consultancy Services Limited, Hadapsar, Pune 411013, India

## Introduction

Human skin consists of numerous tactile receptors present at various depths inside the skin<sup>1-2</sup>. The cutaneous sense in humans comes from different types of sensory receptors known as mechanoreceptors that sense mechanical stimuli like force, vibration, or movement at the surface of the skin<sup>2</sup>. They are classified into two categories; Slow adapting receptors (SA-I and SA-II), which respond to static and quasi-static stimuli - meaning that they produce a sustained response against a stable and constant stimulus; and Fast adapting receptors (FA-I and FA-II) respond to dynamic stimuli such as vibrations<sup>1-2</sup>. These receptors are innervated by special nerve fibres which have different structure and conduction velocity<sup>3</sup>. Figure 1(a) shows the skin mechanoreceptors and nerves innervating these receptors.

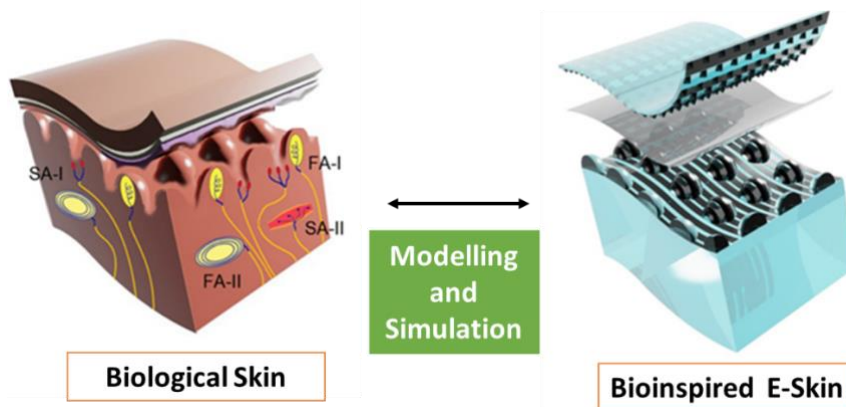


Figure 1: Overview of this report. Inspired by different mechanoreceptors in skin, e-skin sensor's property optimisation was carried out using different modelling and simulation tools. Few parts of this figure were taken from ref<sup>4</sup>

Inspired from the human skin, e-skins or electronic skins are being developed across the world which converts external stimuli into electrical signals. It is desirable to have highly reliable, flexible and sensitive e-skins<sup>1</sup>. To attain such properties, e-skins consist of a wide variety of sensors like pressure, shear, strain, etc which are connected via flexible interconnects as shown in Figure 1(b). These sensors especially pressure and shear sensors act in the same way as individual mechanoreceptors of skin. Depending on the mechanism involved these sensors could be categorized as physical, chemical or biological sensors<sup>5</sup>. However, the material

properties of these sensors and interconnects govern the functioning of these e-skins. In that regard, optimising the material properties using simulation tools is highly beneficial.

## Skin touch mechanism and its mimicking by e-skin sensors

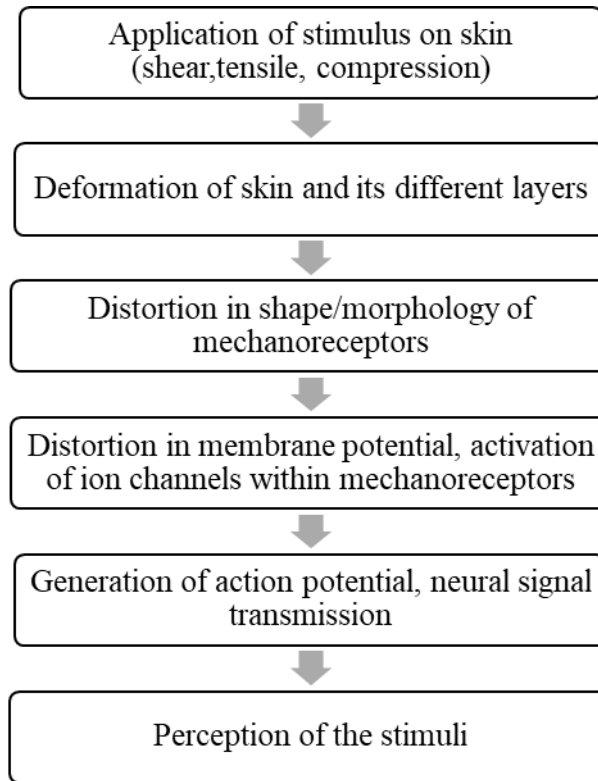


Figure 2: Flowchart of mechanotransduction mechanism in skin<sup>2,6</sup>

Figure 2 shows the flowchart of mechanotransduction mechanism in skin showing how a mechanical stimulus on skin is detected and then converted into electrical signals. Cutaneous mechanoreceptors convey four basic types of information when stimulated— modality (e.g., gentle touch, vibration, stretch, injurious forces), location, intensity, and timing<sup>2-3, 7</sup>. At the receptive site, mechanical energy is transduced into a change in membrane potential that is called receptor potential. The receptor potential is then transformed into a neural pulse code, in which the frequency of action potentials reflects to some extent the amplitude of the receptor potential<sup>6, 8-10</sup>. Similarly, under the action of an external stimuli, certain property like capacitance or resistance change for a capacitive or resistive sensor respectively which is transduced into electrical signal. In this way, e-skin sensors can detect any kind of pressure or strain near its surface.

## Modelling and simulation of e-skin sensors

The recent advent of various simulation approaches and increase in computational power in last two decades have produced quite accurate predictions for virtually most types of material properties and their application in e-skin sensors. Depending on the application (i.e. timescale and lengthscale), various simulation methodologies are employed for optimising the material

properties for e-skin sensors. For example, Molecular dynamics (MD) simulations are mostly used to understand the chemical, diffusion or interfacial phenomena at few nanometers or nanoseconds level while finite element methods (FEM) are used to understand the underlying physics at few micro- to milli- meters or seconds level.

In this regard, we performed property optimisation of pressure and strain sensor using simulation techniques. This report summarises the results from application of multiscale techniques like MD and FEM simulations for optimising and understanding the material properties of strain and pressure sensors. The results shown in this report were published in the references<sup>11-12</sup>.

## MD simulations for understanding the filler-elastomer interactions in soft-flexible strain sensors

Recently, few elastomer composite based piezoresistive strain sensors with high gauge factor were fabricated in our lab<sup>11</sup>. In these sensors, as shown in Figure 3(a), the sensing material consisted of a composite material with ecoflex as the soft elastomer matrix material while graphite and carbon nanotubes(CNT) were added as filler material. The weight ratio for elastomer to graphite to CNT was 1:0.2:0.015. This sensor had high stretchability without showing any micro-cracks (Figure 3(b)) even at high strains but low sensitivity meaning lower change in electrical resistance when tensile strain was applied to this sensor as seen from Figure 3(d). To increase the sensitivity of these sensors, graphene carbon paste (GCP) was added in the composite material with weight of GCP equal to that of ecoflex. The new sensor fabricated showed good sensitivity showing greater change in the electrical resistance but lower stretchability when tensile strain was applied and it showed formation of micro-cracks as shown in Figures 3(c) and 3(d).

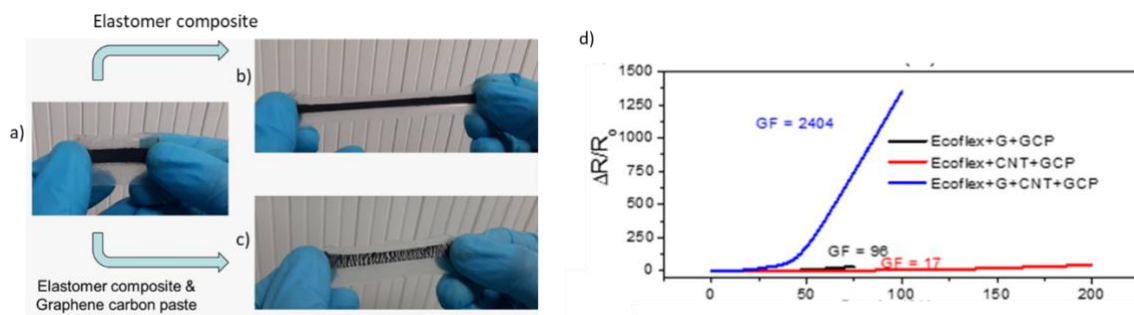


Figure 3: (a) A upstretched strain sensor, (b) Sensor with graphite, CNT and ecoflex as sensing layer under stretched condition, (c) Sensor with graphite, CNT, GCP and ecoflex as sensing layer under stretched condition (d) relative change in resistance for different sensors<sup>11</sup>

For understanding the role of GCP in sensor response and stretchability, molecular dynamics (MD) simulations were carried out on elastomer matrix before and after adding the GCP. MD simulations are the best technique to study the effect of chemical composition and interfaces on mechanical property of sensors at nano-scale level. In these simulations, initially two simulation boxes were made with polydimethylsiloxane (PDMS) molecules acting as the elastomer material. In the first box, 100 chains of PDMS having 15 monomers each, 2 graphene sheets

(having size 5 nm x 5 nm with chirality (3,3) and 2 single-walled carbon nanotubes (SWCNT) (having tube length of 4.92 nm and tube diameter of 0.41 nm with chirality (3,3) were placed inside the box in the weight ratio of 1:0.2:0.015 respectively. In the second box, 4 graphene sheets and 60 C<sub>60</sub> fullerene particles (to mimic the effect of spherical carbon particles present in GCP) were added additionally in the previous system. These extra graphene sheets and fullerene particles were inserted to mimic the properties of GCP used in the experiment and weight ratio was maintained as same as the experiments.

Both the systems were initially minimised. It was then followed by NPT equilibration at 0 atm pressure and 300K temperature for 1 ns with a timestep of 1 fs. Subsequently, these systems were subjected to simulated annealing from 300K to 600K with total annealing time of 1 ns and then they were relaxed at 600K for another 1ns. Further they were cooled down to 300K in another 1 ns and finally they were equilibrated at 300K for 5ns. All the steps for simulated annealing and equilibration were run in NPT ensemble. After equilibration, a tensile test in x-direction was performed for both the systems while keeping the pressure constant in the other two directions at 0 atm. The strain rate of 10<sup>10</sup> s<sup>-1</sup> was applied during the tensile simulations. All these simulations were run in LAMMPS<sup>13</sup> using OPLSAA forcefield parameters.

Figure 4 shows the simulation results for both the sensors and the effect of addition of GCP in the composite material. Nano-voids were observed at strain level of ~70% in the sensor containing GCP which leads to formation of cracks at strain of 110%. However, no cracks were observed for sensor without GCP even at 110% strain. The reason behind the difference in the cracking behaviour could be understood as follows. Because of addition of GCP in the sensor matrix, the amount and density of filler particles in elastomer material increases which further leads to higher particle to particle interactions among the filler particles due to Van der Waals forces resulting in agglomeration of particles. It could be clearly seen that micro cracks were developed perpendicular to the stretching axis. Because of generation of these cracks, the available conductive path for electrons through the filler material decreases which leads to higher increase in resistance in sensors with GCP. However, the sample without GCP or less loading of GCP have relatively small change in resistance due to the availability of more conductive paths in comparison with its counterpart. The observation made from the simulation matched complements well with the experimental results that the addition of GCP contributed to the decrease in stretchability and increase in sensor response.

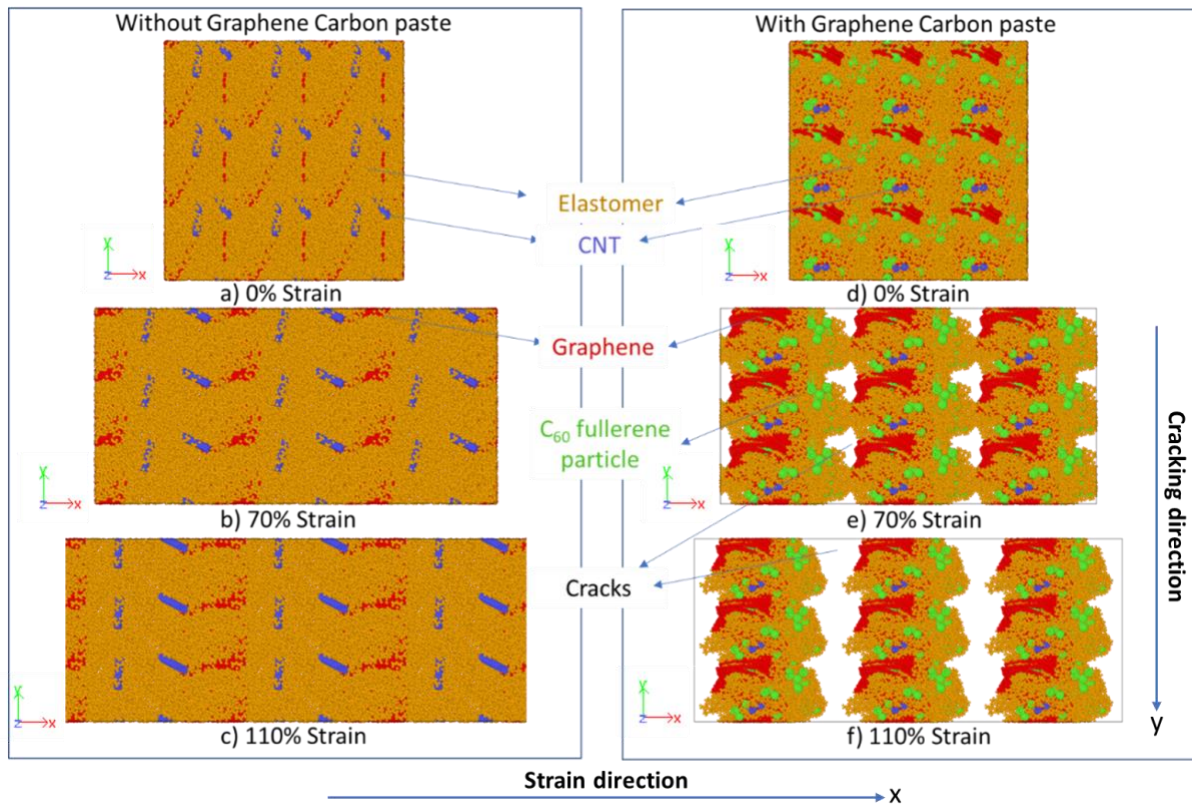


Figure 4: A molecular dynamic simulation for elastomer-GCP-filler composite: (a) without GCP and (b) with GCP<sup>11</sup>

## FEM analysis for design optimisation of piezoelectric nanowires based soft capacitive sensors

Recently, piezoelectric nanowires (NWs) based capacitive pressure sensors have shown promising sensing capabilities<sup>14-15</sup>. Inspired by the design used by Kumaresan et al<sup>5</sup>, design optimisation and effect of piezoelectric effect of ZnO NWs on the sensitivity of pressure sensor using FEM was analysed. FEM is ideal to use in this case because here the length scale of simulations lie in few micrometers which can't be handled properly by methodologies like MD simulations.

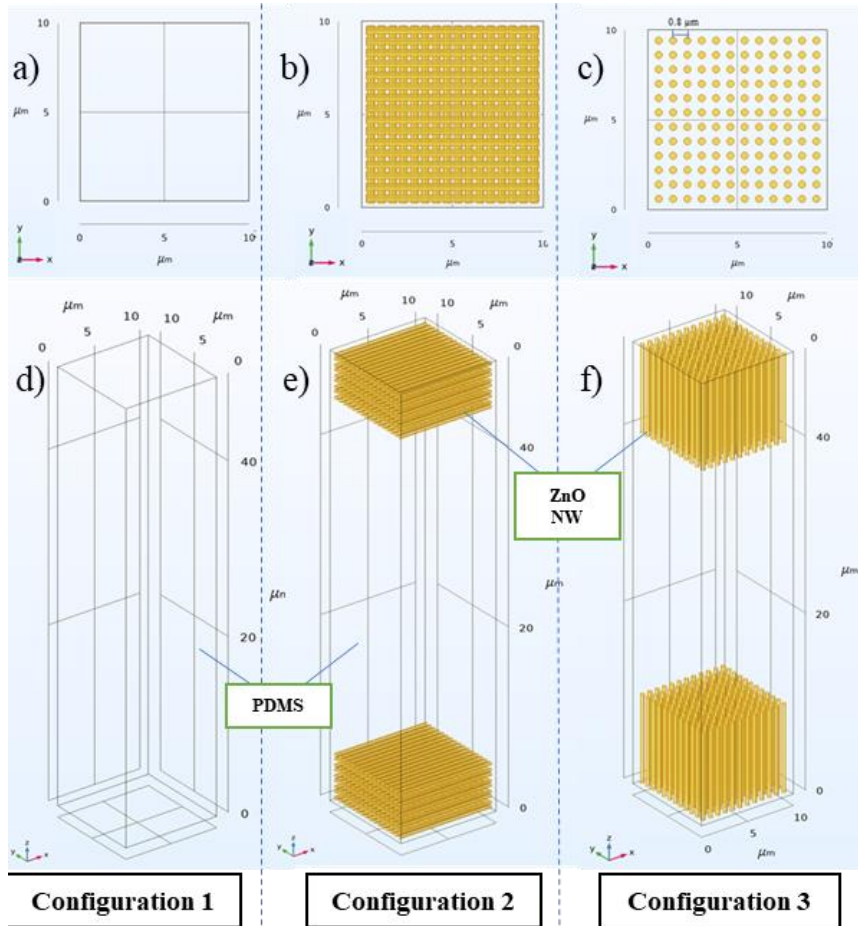


Figure 5: Geometry for three configurations (1, 2 and 3) used in the simulations. (a-c) are top view and (d-f) are their perspective views<sup>12</sup>.

In this study, three designs for the sensors were used, as shown in Figure 5. In the first design, a block of PDMS was taken with dimensions  $10 \mu\text{m} \times 10 \mu\text{m} \times 50 \mu\text{m}$  while in others 144 ZnO NWs were added near to each face in the z-direction. An attempt was also made to understand the effect of addition and orientation of ZnO NWs on the sensor's sensitivity. The radius (R) and length (L) of ZnO NWs were also changed as shown in Table 1 during the simulations to observe the effect of aspect ratio of NWs on the sensitivity of the sensor.

**Table 2:** Configuration and dimensions of different sensors simulated (here P, H1 and V(1-5) stands for PDMS, horizontal and vertical respectively)

Sensor/ Properties	P	H1	V1	V2	V3	V4	V5
Configuration	1	2	3	3	3	3	3
Radius of ZnO NW (in $\mu\text{m}$ )	-	0.2	0.2	0.2	0.2	0.15	0.25
Length of ZnO NW (in $\mu\text{m}$ )	-	9.5	10	5	1	10	10
Aspect Ratio (L:R)	-	47	50	25	5	66	40

In all the simulations, the bottom surface in z- direction was constrained and grounded while pressure was applied and varied from 0-10 kPa on the top surface in negative z-direction. A terminal voltage of 1V was applied on the same top surface. All the simulations were carried out in COMSOL 6.0 and both *Solid Mechanics* and *Electrostatics* modules of COMSOL were coupled together via the *Piezoelectric Effect* Multiphysics. The material properties for PDMS and ZnO NW were taken from the library of COMSOL Multiphysics as these values have been used previously in modelling the same materials. Air was taken as dielectric material outside the sensors and moving mesh method was used to model the interaction between air and the sensors.

The variation in relative change in capacitance in each of the sensor with applied pressure was calculated as  $\% \Delta C/C_0 = (C-C_0) \times 100/C_0$  where C and  $C_0$  are Maxwell's capacitance of the system at any pressure and zero pressure respectively while the sensitivity (S) =  $\Delta(\% \Delta C/C_0)/\Delta P$ , where  $\Delta P$  is the change in pressure or it can be calculated as slope of the  $\% \Delta C/C_0$  vs pressure curve.

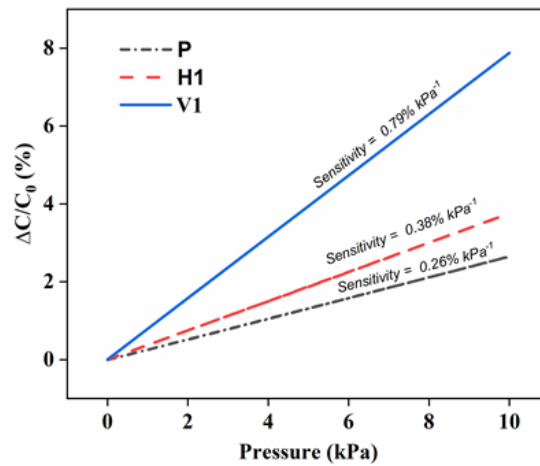


Figure 6: Variation in relative change in capacitance for sensors P, H1 and V1<sup>12</sup>.

Figure 6 shows the relative change in capacitance and sensitivity for sensors P, H1 and V1. The calculated sensitivity for sensor with PDMS only (i.e. P) as dielectric is  $0.26\% \text{ kPa}^{-1}$  which lies within the range of experimentally measured sensitivity ( $0.125\text{-}0.8\% \text{ kPa}^{-1}$ )<sup>5, 16</sup> for capacitive sensors with similar design. When the ZnO NWs were added inside the PDMS near the electrodes, the sensitivity for sensors H1 and V1 increased in comparison to sensitivity of sensor P which shows that addition of ZnO NWs near the electrodes enhances the sensitivity. Also, the level of increase in sensitivity (around 1~3 times) with respect to sensors with PDMS only as dielectric is comparable to the experimentally observed increase (i.e., around 1.3~7 times). It was also observed that the sensitivity is higher in vertical ZnO NWs based sensor compared to horizontal ZnO NWs based sensor. This is due to generation of higher magnitude of piezoelectric polarization in vertical ZnO NWs than horizontal NWs at same pressure as shown in Figure 7.



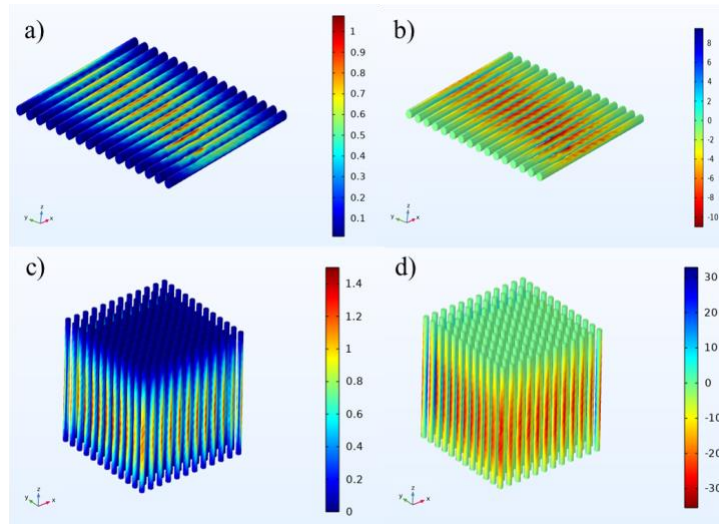


Figure 7: (a) Von Mises stress (in MPa) and (b) piezoelectric polarization (in  $\text{mC}/\text{m}^2$ ) for ZnO NWs closest to the top surface in Sensor H1, (c) von Mises stress (in MPa) and (d) piezoelectric polarization (in  $\text{mC}/\text{m}^2$ ) for ZnO NWs closest to top surface in Sensor V1. All the graphs were plotted at the pressure of  $10 \text{ kPa}^{12}$ .

It was also observed that with decreasing diameter or increasing length or aspect ratio of ZnO NWs as shown in Figure 8 enhanced the sensitivity of the sensor. This happens because the bendability of NWs increases with increasing aspect ratio and thus resulting in larger strain in NWs which leads to generation of higher piezoelectric polarisation within ZnO NWs. Thus, to design a pressure sensor with piezoelectric NWs, based on these simulation results, it is advised to have higher aspect ratio NWs in vertical orientation. However, these simulations have a limitation that it considers non-contacting perfectly oriented NWs which is very difficult to attain in experimental conditions where you achieve some randomness in the orientation and contact between NWs.

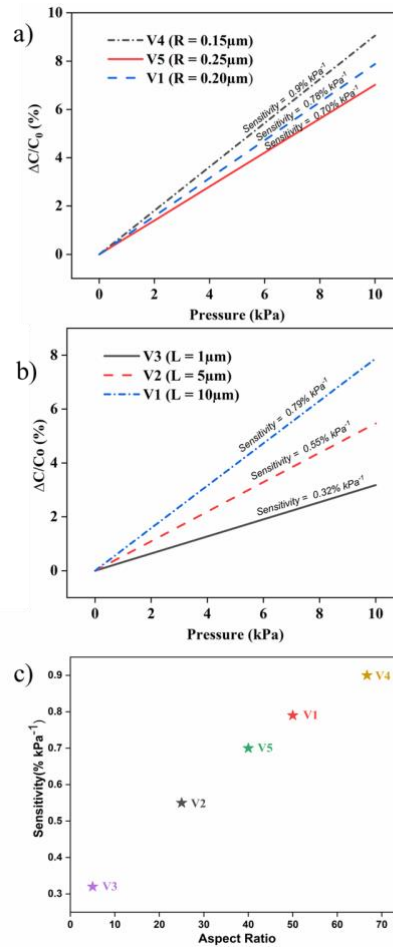


Figure 8: Effect of (a) radius, (b) length and (c) aspect ratio of ZnO NWs on the sensitivity of sensors<sup>12</sup>.

## Conclusion

In above two works, the material properties as well as design of the pressure and strain sensors were optimised using two different methodologies. This shows that multi-scale simulation technologies could benefit in achieving better sensor designs. Based on these works, a computational model for generation and optimisation of signal outputs from network of sensors will be developed in future work. Also, using these simulation tools, we will try to model the behaviour of individual receptors of skin. While MD simulation will be used to study the functioning of mechanically activated ion channels present in various mechanoreceptors, while FEM will be utilised along with other mathematical models to model the output nerve signals from single or population of receptors under the action of an external stimulus. In that way, a complete model of mechano-transduction mechanism of skin will be developed.

## References

1. Dahiya, R.; Yogeswaran, N.; Liu, F.; Manjakkal, L.; Burdet, E.; Hayward, V.; Jörintell, H., Large-area soft e-skin: The challenges beyond sensor designs. *Proceedings of the IEEE* **2019**, *107* (10), 2016-2033.
2. Dahiya, R. S.; Metta, G.; Valle, M.; Sandini, G., Tactile Sensing—From Humans to Humanoids. *IEEE Transactions on Robotics* **2010**, *26* (1), 1-20.
3. Nghiem, B. T.; Sando, I. C.; Gillespie, R. B.; McLaughlin, B. L.; Gerling, G. J.; Langhals, N. B.; Urbanek, M. G.; Cederna, P. S., Providing a Sense of Touch to Prosthetic Hands. *Plastic and Reconstructive Surgery* **2015**, *135* (6).
4. Boutry, C. M.; Negre, M.; Jorda, M.; Vardoulis, O.; Chortos, A.; Khatib, O.; Bao, Z., A hierarchically patterned, bioinspired e-skin able to detect the direction of applied pressure for robotics. *Science Robotics* **2018**, *3* (24), eaau6914.
5. Kumaresan, Y.; Ma, S.; Ozioko, O.; Dahiya, R., Soft Capacitive Pressure Sensor with Enhanced Sensitivity assisted by ZnO NW Interlayers and Airgap. *IEEE Sensors Journal* **2022**, 1-1.
6. Geffeney, S. L.; Goodman, M. B., How we feel: ion channel partnerships that detect mechanical inputs and give rise to touch and pain perception. *Neuron* **2012**, *74* (4), 609-19.
7. Ozioko, O.; Dahiya, R., Smart Tactile Gloves for Haptic Interaction, Communication, and Rehabilitation. *Advanced Intelligent Systems* **2021**, *n/a* (n/a), 2100091.
8. Abraira, V. E.; Ginty, D. D., The sensory neurons of touch. *Neuron* **2013**, *79* (4), 618-639.
9. Handler, A.; Ginty, D. D., The mechanosensory neurons of touch and their mechanisms of activation. *Nat Rev Neurosci* **2021**, *22* (9), 521-537.
10. Zimmerman, A.; Bai, L.; Ginty David, D., The gentle touch receptors of mammalian skin. *Science* **2014**, *346* (6212), 950-954.
11. Kumaresan, Y.; Mishra, S.; Ozioko, O.; Chirila, R.; Dahiya, R., Ultra-High Gauge Factor Strain Sensor with Wide-Range Stretchability. *Advanced Intelligent Systems* **2022**, *n/a* (n/a), 2200043.
12. Mishra, S.; Baghini, M. S.; Shakthivel, D.; Rai, B.; Dahiya, R. In *Sensitivity Analysis of ZnO NWs Based Soft Capacitive Pressure Sensors using Finite Element Modeling*, 2022 IEEE International Conference on Flexible and Printable Sensors and Systems (FLEPS), 10-13 July 2022; 2022; pp 1-4.
13. Thompson, A. P.; Aktulga, H. M.; Berger, R.; Bolintineanu, D. S.; Brown, W. M.; Crozier, P. S.; in 't Veld, P. J.; Kohlmeyer, A.; Moore, S. G.; Nguyen, T. D.; Shan, R.; Stevens, M. J.; Tranchida, J.; Trott, C.; Plimpton, S. J., LAMMPS - a flexible simulation tool for particle-based materials modeling at the atomic, meso, and continuum scales. *Computer Physics Communications* **2022**, *271*, 108171.
14. Nguyen, T. D.; Lee, J. S., Recent Development of Flexible Tactile Sensors and Their Applications. *Sensors (Basel)* **2021**, *22* (1).

15. Zhou, J.; Gou, X.; Fan, D.; Wang, J.; Wan, Z., Polydimethylsiloxane/BaTiO<sub>3</sub> Nanogenerators with a Surface-Assembled Mosaic Structure for Enhanced Piezoelectric Sensing. *ACS Applied Materials & Interfaces* **2022**, *14* (33), 38105-38115.

16. Ma, S.; Kumaresan, Y.; Ozioko, O.; Dahiya, R. In *Highly Sensitive Flexible Capacitive Pressure Sensor with ZnO NW interlayers*, 2021 IEEE International Conference on Flexible and Printable Sensors and Systems (FLEPS), 20-23 June 2021; 2021; pp 1-4.